Pressure-induced Breaking of Equilibrium Flux Surfaces in the W7AS Stellarator

A. Reiman, M.C. Zarnstorff, D. Monticello
Princeton Plasma Physics Laboratory, Princeton, NJ 08543 USA
email address of main author*:* reiman@pppl.gov

A. Weller, J. Geiger, and the W7-AS Team
Max-Planck Institute for Plasma Physics, EURATOM Assoc., D-17491 Greifswald, Germany

Abstract. Calculations are presented for two shots in the W7AS stellarator which differ only in the magnitude of the current in the divertor control coil, but have very different values of experimentally attainable β (⟨β⟩ ≈ 2.7% vs. ⟨β⟩ ≈ 1.8%). Equilibrium calculations find that a region of chaotic magnetic field line trajectories fills approximately the outer 1/3 of the cross section in each of these configurations. The field lines in the stochastic region are calculated to behave as if the flux surfaces are broken only locally near the outer midplane and are preserved elsewhere. The calculated magnetic field line diffusion coefficients in the stochastic regions for the two shots are consistent with the observed differences in the attainable β, and are also consistent with the differences in the reconstructed pressure profiles.

1. Introduction

It has been an open question since the early days of the fusion program whether flux surfaces are lost in high β stellarator equilibria.[1] There have been a number of theoretical papers on the subject (see Refs. 2 and 3, Ref. 4 and references therein), and two equilibrium codes have been developed that can handle magnetic islands and stochastic regions.[5,6] Only in recent years have stellarators achieved values of β sufficiently high to study the issue experimentally. Both the W7AS and LHD stellarators exhibit degraded confinement at high values of β that does not appear to be caused by instabilities,[7,8] There is no diagnostic in these experiments that directly indicates whether surfaces are broken. In this paper we compare experimental observations on the W7AS stellarator with PIES code calculations to investigate this issue. We focus on two shots that are of particular interest in this regard.

The equilibrium calculations described here exhibit large regions of chaotic magnetic field line trajectories. As discussed in Section 3, equilibrium reconstruction indicates the presence of substantial pressure gradients in the stochastic regions. As discussed in Section 4, the calculation of equilibria for these cases poses several subtleties, including the issue of how to handle magnetic differential equations along chaotic field line trajectories. The equilibrium calculations find that the magnitude of the pressure gradient in the stochastic region can strongly influence the width of the stochastic region.

Some calculations for the W7AS shots studied here were presented in Ref. 7. That study has been extended here to examine the structure of the magnetic field in the stochastic region (Section 5), and the diffusion coefficient of the magnetic field lines (Section 6), providing a more direct comparison of the calculations with experimental observations. Also, relative to the earlier calculations for these shots, the equilibrium reconstruction has been extended to use magnetics measurements for reconstructing the current profile (Section 3), and the modeling of the equilibrium in the stochastic region has been improved (Section 4).

Section 2 of this paper describes the W7AS shots studied here. The VMEC equilibrium reconstruction for these shots is described in Section 3. Section 4 describes the subtleties posed by the finite pressure gradient in the edge stochastic region, and how they are handled

in the PIES code calculations. Section 5 describes the novel structure of the magnetic field line trajectories in the stochastic region. Section 6 describes the calculation of the magnetic field line diffusion coefficient and comparison with W7AS experimental observations. Finally, Section 7 presents some conclusions.

2. W7AS Divertor Control Coils and their Effect on β

W7AS has a set of divertor control coils which were designed to provide control over the resonant magnetic field near the plasma edge, for control of the edge islands in studies of island divertors. The coils have been calculated to have little effect on the vacuum field rotational transform profile, on the neoclassical ripple transport,[7] or on the vacuum field magnetic axis shift.

The vacuum magnetic fields corresponding to the shots we study here have $\iota \approx ½$ at the edge, and the configuration is bounded by a well defined set of islands when the divertor control coil current $I_{cc} = 0$. These vacuum edge islands can be suppressed by a divertor control coil current $I_{cc} = -0.7$ kA, so that the field then has nested flux surfaces out to the divertor plates. This suggested the use of the control coils in high β shots to provide a larger volume of nested flux surfaces, potentially allowing the machine to achieve higher values of β.

Figure 1 shows the maximum $\langle\beta\rangle$ achieved in four W7AS shots which differed only in the magnitude of the divertor control coil current. The highest $\langle\beta\rangle$ was achieved at a value of $I_{CC} / I_M \approx 0.15$, corresponding to $I_{CC} \approx -2.5$ kA, over three times the current that produces the largest flux surface volume at $\beta = 0$. The imposition of this large control coil current in the vacuum field produces a set of large islands at the edge whose phase is opposite to those where $I_{cc} = 0$. We have used the PIES code[5] to study the finite β effects that determine the optimal value of I_{CC}.

3. W7AS Modeling using Experimentally Determined Pressure and Current Profiles

For the initial step in the modeling, a modified version of the STELLOPT code[10] was used to calculate an optimized equilibrium reconstruction[7] based on the VMEC[11] three-dimensional equilibrium code, which assumes nested flux surfaces. Given specified coil currents, VMEC was used to calculate corresponding free-boundary equilibria for candidate pressure and current profiles, and a set of corresponding diagnostic data was calculated for comparison with the experimental data. The pressure and current profiles of the equilibria were adjusted to optimize the fit to the Thomson scattering data as well as to the data from the magnetic diagnostics. Earlier modeling of the two shots examined in this paper assumed zero net current within each flux surface, and optimized the fit to the Thomson data.[7] To obtain an adequate fit also to the data from the magnetic diagnostics, it is necessary to allow a finite net current, and to adjust its profile accordingly.

The VMEC equilibrium solution was used as the starting point for the calculation with the PIES code, which does not assume good flux surfaces. Having found the pressure and current profiles that provide an optimal fit to the experimental data, we keep these profiles fixed as the PIES code iterates, even when large stochastic regions appear at the plasma edge. In order to do that, we need to develop an appropriate equilibrium model for the stochastic regions.

4. Plasma Equilibrium in Regions of Chaotic Magnetic Field Line Trajectories

We assume that the magnetic field consists of two pieces, a piece with good flux surfaces, plus a perturbation that produces chaotic field line trajectories and causes the magnetic field lines to slowly diffuse relative to the unperturbed flux surfaces. The perturbation contributes to transport, but it is assumed to have only a small effect on the shape of the isobaric surfaces.

The MHD force balance equation, $\mathbf{j}\times\mathbf{B}=\nabla p$, implies that $\mathbf{B}\cdot\nabla p=0$, which in turn implies that the pressure gradient must vanish in a stochastic region. The W7AS equilibrium reconstructions suggest that there are finite pressure gradients in the stochastic regions, and we cannot satisfy the MHD equilibrium equations per se. However, consider a tensor pressure, $\boldsymbol{P} = p\boldsymbol{1} + \boldsymbol{\pi}$, with $|\nabla\cdot\boldsymbol{\pi}| << \nabla p$. We also allow for a weak flow, with $|\rho\mathbf{v}\cdot\nabla\mathbf{v}| << |\nabla p|$. The force-balance equation is

$$\mathbf{j}\times\mathbf{B} - \rho\mathbf{v}\cdot\nabla\mathbf{v} - \nabla\cdot\pi = \nabla p\,.$$

Taking the dot product of **B** with the force balance equation we get

$$\mathbf{B}\cdot\nabla p = -\mathbf{B}\cdot(\rho\mathbf{v}\cdot\nabla\mathbf{v} + \nabla\cdot\pi)\,.$$

If the field lines diffuse slowly relative to the unperturbed flux surfaces, the pressure gradient along the field lines is small, and it can be balanced by the small terms on the right-hand side of the equation. We assume that the plasma velocity along the magnetic field lines adjusts itself to satisfy this equation. The solution of the equation along the field lines can be regarded as part of the transport problem, and we will see that it does not enter into the self-consistent solution for the equilibrium magnetic field using the other components of the force balance equation.

Taking the cross product of **B** with the force balance equation we obtain an expression for $\mathbf{j}_\perp$, the component of the current density perpendicular to the magnetic field,

$$\mathbf{j}_\perp = \mathbf{B}\times\nabla p / B^2 + \mathbf{B}\times(\nabla\cdot\boldsymbol{\pi}+\rho\mathbf{v}\cdot\nabla\mathbf{v})/B^2 \approx \mathbf{B}\times\nabla p / B^2\,. \qquad (1)$$

The component of **j** parallel to the magnetic field, $j_{||}$, is determined from $\nabla\cdot\mathbf{j}=0$, which gives the 1D equation along the field line ("magnetic differential equation")

$$\mathbf{B}\cdot\nabla(j_{||}/B) = -\nabla\cdot\mathbf{j}_\perp\,. \qquad (2)$$

The equations are closed by Ampere's Law: $\nabla\times\mathbf{B}=\mathbf{j}$. Equations (1) and (2) specify **j** as a function of **B**, **j** = **j**(**B**). With Ampere's Law, we have a self-consistent set of equations that can be solved for the equilibrium magnetic field without reference to the force balance along the magnetic field. We have recast the equilibrium equations in the form

$$\nabla\times\mathbf{B} = \mathbf{j}(\mathbf{B})\,. \qquad (3)$$

This is the form in which the equations are solved by the PIES code.

In practice, Eq. (1) gives an explicit expression for $\mathbf{j}_\perp$, and Eq. (3) can be solved by inverting a matrix which represents the curl operator. (We finite difference in the radial direction and use a Fourier representation in the θ and ϕ directions.) The magnetic differential equation, Eq. (2), presents subtle issues, particularly when the field line trajectories are chaotic. We first discuss the case with good flux surfaces, and then turn to the difficulties posed by chaotic field line trajectories.

On a good flux surface, Eq. (2) can be solved by transforming to magnetic coordinates.[12,13] ("Magnetic coordinates" are flux coordinates with straight field lines: $\mathbf{B}\cdot\nabla\psi=0$; $\mathbf{B}\cdot\nabla\theta/\mathbf{B}\cdot\nabla\phi$ constant on the flux surface = $\iota(\psi)$.) Let $\mu\equiv j_{||}/B$. In magnetic coordinates Eq. (2) can be rewritten

$$\frac{\partial \mu}{\partial \phi} + \iota \frac{\partial \mu}{\partial \theta} = -\frac{\nabla \cdot \mathbf{j}_\perp}{B^\phi}, \; B^\phi \equiv \mathbf{B} \cdot \nabla \phi \,. \tag{4}$$

Fourier transforming in θ and ϕ gives

$$(nN - \iota m)\mu_{nm} = -(\frac{\nabla \cdot \mathbf{j}_\perp}{B^\phi})_{nm}, \tag{5}$$

where n is the toroidal mode number per period, N is the number of periods, and m is the poloidal mode number. Some care must be exercised to calculate the near-resonant components accurately.[12] The $m = 0$, $n = 0$ Fourier coefficient, μ_{00}, is determined by the constant of integration for Eq. (4), which is determined by the profile of the net current.

In a stochastic magnetic field, Eq. (4) picks up additional terms:

$$\frac{\partial \mu}{\partial \phi} + \iota(\psi) \frac{\partial \mu}{\partial \theta} + \frac{\delta B^\psi}{B^\phi} \frac{\partial \mu}{\partial \psi} + \frac{\delta B^\theta}{B^\phi} \frac{\partial \mu}{\partial \theta} = -\frac{\nabla \cdot \mathbf{j}_\perp}{B^\phi} \,. \tag{6}$$

Here we have separated the magnetic field into two pieces, a piece with good flux surfaces, plus a perturbation $\boldsymbol{\delta}\mathbf{B}$ that produces chaotic field line trajectories. We have used the notation $\delta B^\psi \equiv \mathbf{B} \cdot \nabla \psi$, $\delta B^\theta \equiv \mathbf{B} \cdot \nabla \theta$. The corresponding homogeneous equation is mathematically equivalent to the 1D collisionless Vlasov equation in the presence of turbulence[14] if we assume that ι is monotonic in the region of interest so that we can adopt it as our radial variable, and we identify $\mu \to f$, $\phi \to t$, $\iota \to$ v, $\theta \to$ x. The $\delta B^\psi / B^\phi$ term is identified with the force parallel to the magnetic field line due to the turbulent electric field, and the $\delta B^\theta / B^\phi$ term is identified with the turbulent $\mathbf{E} \times \mathbf{B}$ term in the Vlasov equation.

The relationship of Eq. (6) to the perturbed Vlasov equation in the presence of turbulence allows us to use resonance-broadening theory as a guide in handling Eq. 6. (See e.g. Ref. [14] and references therein.) The wavelength along the field line of a mode having mode numbers (n,m) is $2\pi R/(nN\text{-}\iota m)$. For near-resonant modes ($nN\text{-}\iota m$ small), the mode has a long wavelength along the field line, and the diffusion of the field line with respect to ι broadens the resonance and eliminates the singularity. For modes that are far from resonance ($nN\text{-}\iota m$ large), the wavelength along the field line is short, and the slow radial diffusion of the field line can be neglected, recovering Eq. (5).

Explicit solutions to Eq. (6) are known only for special cases. In the W7AS equilibrium calculations discussed in this paper, the resonant Fourier components have relatively high mode number because the toroidal mode number must be a multiple of the number of periods (5 for W7AS). At ι = 0.5, for example, the lowest order resonant equilibrium Fourier coefficient is $n = 5$, $m = 10$. The high mode number, near-resonant Fourier coefficients of the equilibrium current density are small, except possibly near the resonant surface. In this context, the resonance broadening plays the role of keeping the amplitude of the resonant components small. We find that the calculation is insensitive to the precise form of the resonance broadening. In other contexts, resonance-broadening is often modeled by $1/\mathrm{x} \to \mathrm{x} / (\mathrm{x}^2 + \varepsilon^2)$. For purposes of our computation, we find it more convenient to use a somewhat different model. The model will be described in Section 5, after we examine the structure of the magnetic field lines in the stochastic region.

The relationship between Eq. (6) and the perturbed Vlasov equation in the presence of turbulence, and the corollaries for equilibria in stochastic magnetic fields, are discussed in more detail in reference [15].

5. Equilibrium Solutions and Chaotic Field Line Trajectories

Figures 2 and 3 show Poincare plots for the PIES equilibrium solutions with I_{cc} = -2.5kA and I_{cc} = 0 respectively. In each case we find a large stochastic region. Although the value of $\langle\beta\rangle$ is substantially higher in the I_{cc} = -2.5kA shot ($\langle\beta\rangle \approx 2.7\%$ vs. $\langle\beta\rangle \approx 1.8\%$), the width of the stochastic region is approximately the same in the two cases. The last nested flux surface is at $r/a \approx 0.65$ in Fig. 2, and at $r/a \approx 0.62$ in Fig. 3, where r/a is measured along the outer midplane at $\phi = 0$ from the magnetic axis. The plasma boundary is at r/a = 1.0.

In the equilibrium calculations, we find that the width of the stochastic region is strongly influenced by the magnitude of the pressure gradient in that region. If we flatten the pressure profile in the stochastic region, the width of that region continues to increase as the code iterates, and the equilibrium is lost.

Ref. 7 reported on the calculation of two sequences of equilibria using the reconstructed pressure profiles for the two shots with a varying multiplier to vary β, and assuming zero net current inside each VMEC flux surface. It was found that the widths of the edge stochastic regions decrease with decreasing β, going to zero below a β threshold. The calculations found that the width of the stochastic region is smaller for the I_{cc} = -2.5kA configuration for each value of β. Also, the β threshold at which the width of the stochastic region goes to zero is larger for that case.

To examine the chaotic field line trajectories, we plot polar coordinates ρ and θ as a function of ϕ along the field lines. The (ρ, θ) coordinate system used for this purpose has been defined in terms of the equilibrium solution obtained by the VMEC code, which uses a representation for the magnetic field that assumes nested flux surfaces. The radial coordinate ρ is taken to be constant on VMEC flux surfaces, and to measure the distance of the VMEC flux surface from the magnetic axis along the $\theta = 0$ $\phi = 0$ line, normalized to equal 1.0 at the boundary of the computational grid. ($\rho \approx 0.95$ at the plasma boundary.) The angular coordinate θ is identical to the VMEC angular coordinate, with $\theta = 0$ on the inner midplane. (The VMEC coordinates are flux coordinates, but they are not magnetic coordinates. They do not make $\mathbf{B}\cdot\nabla\theta / \mathbf{B}\cdot\nabla\phi$ constant on the flux surfaces.)

Figure 4 shows plots of ρ and θ vs.ϕ for the I_{cc} = -2.5kA, $\langle\beta\rangle \approx 2.7\%$ configuration. Figure 4a shows a relatively smooth curve punctuated by rapid, erratic radial excursions. The field line following was terminated when one of the large radial excursions caused the field line to exit the plasma. Figure 5 shows ρ vs.ϕ for a field line lying on a flux surface. The plot does not exhibit such radial jumps, and the radial excursion of the trajectory remains bounded.

The abrupt radial excursions in Fig.4a occur when the field line crosses the outboard midplane, $\theta = \pi$. To demonstrate this, Fig. 6 shows the same ρ vs.ϕ plot as Fig. 4a, with additional vertical lines placed at the crossings of the outer midplane. It can be seen that the radial jumps occur only near the outer midplane, and that, furthermore, erratic behavior occurs each time the trajectory crosses the outer midplane. The value of ρ on each smooth segment of the curve between the radial jumps returns to approximately its initial value as the

field line returns to the $\theta = \pi$ region. The behavior of the field line shown in Figs. 4 and 6 is typical of the field lines in the stochastic region. The field lines behave as if, in effect, the flux surfaces in the stochastic region have been punctured near the outer midplane but remain intact elsewhere. This differs from the picture conventionally assumed for regions of chaotic magnetic field lines, where the field lines are everywhere diffusing radially. (See, e.g., [9].) The calculations are consistent with the widespread expectation in the stellarator community that equilibrium flux surfaces are broken at high β by the strong compression and distortion of the magnetic flux surfaces near the outer midplane caused by the Shafranov shift. The surface remnants are different from cantori, which are remnants of special surfaces with noble magnetic winding number. Unlike cantori, the behavior we observe has been exhibited by all of the chaotic magnetic field line trajectories we have studied in W7AS equilibria. Note that the narrowness in ϕ of the region where erratic behavior occurs is enhanced by the fact that the field line trajectory moves rapidly through the $\theta = \pi$ region, as can be seen in Fig. 4b. Also, the increased magnitude of the ρ excursions near the outer midplane is due in part to the fact that the distance between the flux surfaces becomes smaller near the outer midplane, so that a small radial excursion in real space gives a larger excursion in ρ. However, the erratic, unbounded behavior of the large excursions is seen only in the stochastic region, where the field lines ultimately are carried out of the plasma.

With this additional information about the chaotic field line trajectories, we revisit the calculation of Pfirsch-Schlüter currents discussed in the previous section. The field lines approximately follow the unperturbed surfaces, except near the outer midplane. The wavelength along the field line of a mode having mode numbers (n,m) is $2\pi R/(nN-\imath m)$. The connection length between encounters with the outer midplane is $2\pi R/\iota$. For Fourier modes having wavelength short compared to the connection length, it is reasonable to do a local analysis, as in Eq. (5). For modes having wavelength long compared to the connection length, phase mixing gives the corresponding solutions of Eq. (6) a small amplitude. Thus we recover the resonance-broadening effect discussed earlier.

As discussed in Section 4, the resonant Fourier components have relatively high mode number in the W7AS equilibrium calculations described in this paper. The high mode number, near-resonant Fourier coefficients of the equilibrium current density are small, except possibly near the resonant surface. In this context, the resonance broadening plays the role of keeping the amplitude of the resonant components small. We find that the calculation is insensitive to the precise form of the resonance broadening.

To implement the resonance-broadening effect in our calculations, we modify the Fourier components of μ on each surface in the stochastic region by multiplying by a factor which is a function of the wavelength of the mode along the field line, is equal to 1 when the wavelength along the field lines is less than the autocorrelation length of the phase, and goes to zero when the wavelength is twice this value.. Letting $\alpha \equiv \left| (nN-\imath m)/\imath \right|$, the factor $f(\alpha)$ used for this purpose is $f(\alpha) = 1$ for $\alpha < 1$, $f(\alpha) = .5\{1 + \cos[(\alpha-1)\pi]\}$ for $1<\alpha<2$, $f(\alpha) = 0$ for $\alpha>2$.

6. Magnetic Field Line Diffusion Coefficient

The magnetic diffusion coefficient measures the mean square radial displacement of a magnetic field line as a function of the distance along the field line. Given the characterization of the chaotic field line trajectories developed in the previous section, we can estimate the magnetic diffusion coefficient as $D_{\mathrm{M}} \approx \left\langle (\Delta r)^2 \right\rangle / L_c$, where L_c is the distance between encounters with

the outer midplane, and $\left\langle (\Delta r)^2 \right\rangle$ is the mean square radial jump experienced by a field line as it crosses the outer midplane. We evaluate this quantity for a given value of ρ by following 100 field lines launched at different values of ϕ once around the torus in the poloidal direction, and measuring the radial jump relative to the underlying unperturbed flux surfaces. (We have verified that increasing the number of field lines followed by a factor of 10 does not have an appreciable effect on the calculated diffusion coefficient.) Fig 7 is a plot of the calculated magnetic diffusion coefficient for the two shots we are studying, in units of meters (= meter^2/meter). The diffusion coefficient is substantially larger for the shot with $I_{CC} = 0$ than for that with $I_{CC} \approx$ -2.5 kA. This is consistent with the observation that the latter shot achieves a higher value of ⟨β⟩ than the former for the same injected neutral beam power.

Figure 8 shows the reconstructed pressure profiles for the two shots. Near the edge, in the region where the field lines are calculated to be stochastic, the reconstructed pressure gradient for $I_{CC} = 0$ is much smaller than that for $I_{CC} \approx$ -2.5 kA. This is again consistent with the picture that the relatively larger magnetic diffusion coefficient for $I_{CC} = 0$ is having a deleterious effect on confinement.

7. Discussion and Conclusions

It has been an open question whether flux surfaces are lost in high β stellarator equilibria. The comparison between experimental observations and three-dimensional equilibrium calculations presented in this paper provides evidence that flux surfaces have been broken over a significant fraction of the cross-section in high β shots of the W7AS stellarator, and that this effect has played a role in limiting the achievable β.

W7AS experiments have found that the magnitude of the divertor control coil current has a strong effect on the achievable β. There is no evidence that instabilities are playing a role in degrading the plasma confinement in these experiments. The divertor control coil has been designed to provide control over the resonant magnetic field near the plasma edge, and it is calculated to have little effect on ι, on neoclassical ripple transport, or on the magnetic axis shift of the vacuum field.

Three-dimensional equilibrium calculations for W7AS find that a region of chaotic field line trajectories emerges at the plasma edge when β exceeds a threshold, and that the stochastic region increases in width as β is increased. Equilibrium reconstruction indicates the presence of a substantial pressure gradient in the stochastic region. In the three-dimensional equilibrium calculations, we find that the width of the stochastic region is strongly influenced by the magnitude of the pressure gradient in that region. If we flatten the pressure profile in the stochastic region, the width of that region continues to increase as the code iterates, and the equilibrium is lost.

The equilibrium calculations are consistent with a simplified, analytically tractable model of flux surface breaking studied in Ref. 2. The magnetic field is represented as the sum of a magnetic field having nested flux surfaces plus a perturbation. Letting (ψ, θ_m, ϕ_m) be the magnetic coordinates for the component of the field having nested surfaces, breaking of the flux surfaces by the perturbation is determined by the magnitude of the resonant Fourier components of $\mathbf{B}\cdot\nabla\psi / \mathbf{B}\cdot\nabla\phi_m$, evaluated in magnetic coordinates. Expressing θ_m-θ and ϕ_m-ϕ as a Fourier series in the geometric angles θ and ϕ, the localized strengthening of $\mathbf{B}\cdot\nabla\theta$ near the

outer midplane associated with the Shafranov shift produces a broadening of the spectrum of θ_m-θ and/or ϕ_m-ϕ. This in turn produces a broadening of the $\mathbf{B}\cdot\nabla\psi/\mathbf{B}\cdot\nabla\phi_m$ spectrum in magnetic coordinates, coupling low order nonresonant Fourier components intrinsic to the stellarator configuration to high order resonant Fourier components and increasing the magnitude of the resonant Fourier components.

Calculations of the magnetic diffusion coefficients in the stochastic regions for the two shots are consistent with the observed differences in the attainable beta, and are consistent with the differences in the reconstructed pressure profile for the two shots. The calculated diffusion coefficient is substantially larger for the shot with $I_{CC} = 0$ than for that with $I_{CC} \approx -2.5$ kA. The reconstructed pressure gradient for $I_{CC} = 0$ is much smaller than that for $I_{CC} \approx -2.5$ kA near the edge, in the region where the field lines are calculated to be stochastic.

Acknowledgment

We are grateful to J. Krommes for valuable discussions concerning resonance-broadening theory and its connection with the calculation of Pfirsch-Schlüter currents in stochastic magnetic fields. This work was supported by DOE contract DE-AC02-76CH03073.

References

[1] L. Spitzer, Phys. Fluids **1**, 253 (1958).
[2] A. H. Reiman and A. H. Boozer, Phys. Fluids 27, 2447 (1984).
[3] J. R. Cary and M. Kotschenreuther Phys. Fluids 28, 1392 (1985).
[4] A. Bhattacharjee, T. Hayashi, C. C. Hegna, et al, Phys. Plasmas **2,** 883 (1995).
[5] A. Reiman and H. Greenside, Compt. Phys. Commun. **43**, 157 (1986).
[6] Harafuji, K., et al., J. Comput. Phys. **81** (1989) 169; Hayashi, T., et al., Phys. Fluids B **2** (1990) 326.
[7] M.C. Zarnstorff *et al*, in Fusion Energy 2004 (Proc. 20th Int. Conf. Vilamoura, 2004) (Vienna: IAEA) CD-ROM EX/3-4 and http://www-naweb.iaea.org/napc/physics/fec/fec2004/datasets/index.html.
[8] A. Weller *et al*, Fusion Science and Technology 50 (2006) 158-170.
[9] A. Rechester and M. Rosenbluth, Phys. Rev. Lett. **40**, 38 (1978).
[10] S. P. Hirshman, D. A. Spong, J. C. Whitson, V. E. Lynch, D. B. Batchelor, B. A. Carreras, J. A. Rome, Phys Rev Letters 80 (528) 1998.
[11] S.P. Hirshman et al., Comput. Phys. Commun. **43** (1986) 143.
[12] A. H. Reiman and H. S. Greenside, J. Comput. Phys. **75,** 423-443 (April 1988).
[13] A. H. Reiman} and N. Pomphrey, J. Comput. Phys. **94**, 225-249 (May 1991).
[14] J. Krommes, Phys. Reports **360**, 1 (2002),.
[15] A. Reiman and J. Krommes, to be published.

Figure Captions

FIG. 1. Variation of achievable ⟨β⟩ versus the divertor control-coil current I_{CC} normalized by the modular coil current, for B=1.25 T, P_{NB} = 2.8 MW absorbed and ι_{vac} = 0.44. The dashed line has been drawn through the data points to guide the eye.

FIG 2.Poincare plots for equilibrium solutions with I_{cc} = -2.5kA, ⟨β⟩ ≈ 2.7%.

FIG 3.Poincare plots for equilibrium solutions with I_{cc} = 0, ⟨β⟩ ≈ 1.8%.

FIG. 4. (a) ρ vs.ϕ, and (b) θ vs.ϕ along a chaotic field line trajectory. ρ ≈ 0.95 on plasma boundary.

FIG. 5. ρ vs.ϕ for a field line lying on a flux surface.

FIG. 6. Plot of fig. 4a, with vertical lines added at crossings of outer midplane.

FIG. 7. Calculated magnetic diffusion coefficient as a function of ρ/a, in units of m (=m^2/m). The radial coordinate here is normalized to equal 1.0 at the plasma boundary (a ≈ .95).

FIG. 8. Reconstructed pressure profiles for (a) I_{cc} = -2.5kA,⟨β⟩ ≈ 2.7%, (b) I_{cc} = 0, ⟨β⟩ ≈ 1.8%.

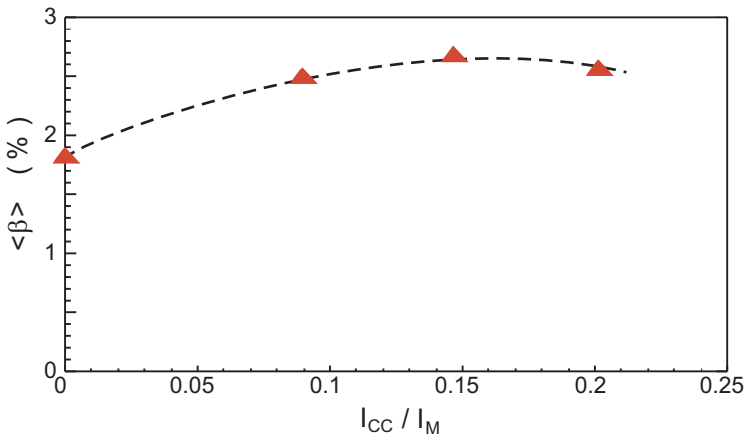

Fig. 1

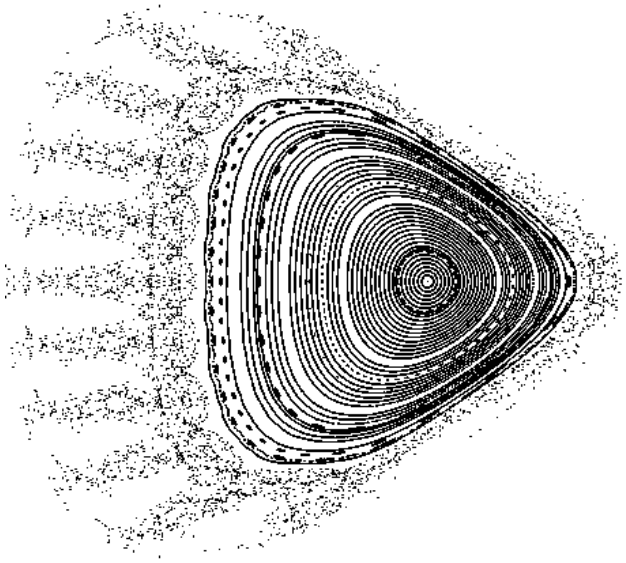

Fig. 2

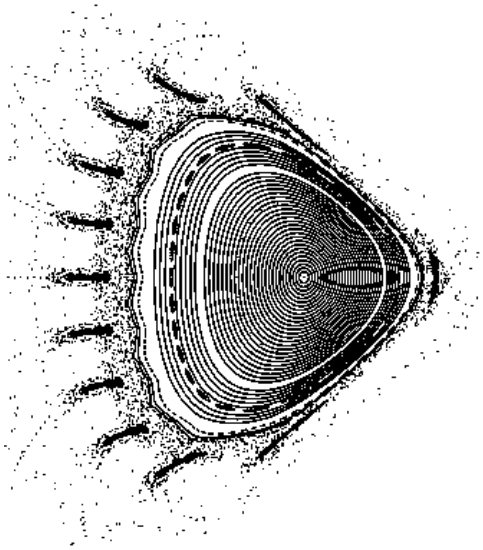

Fig. 3

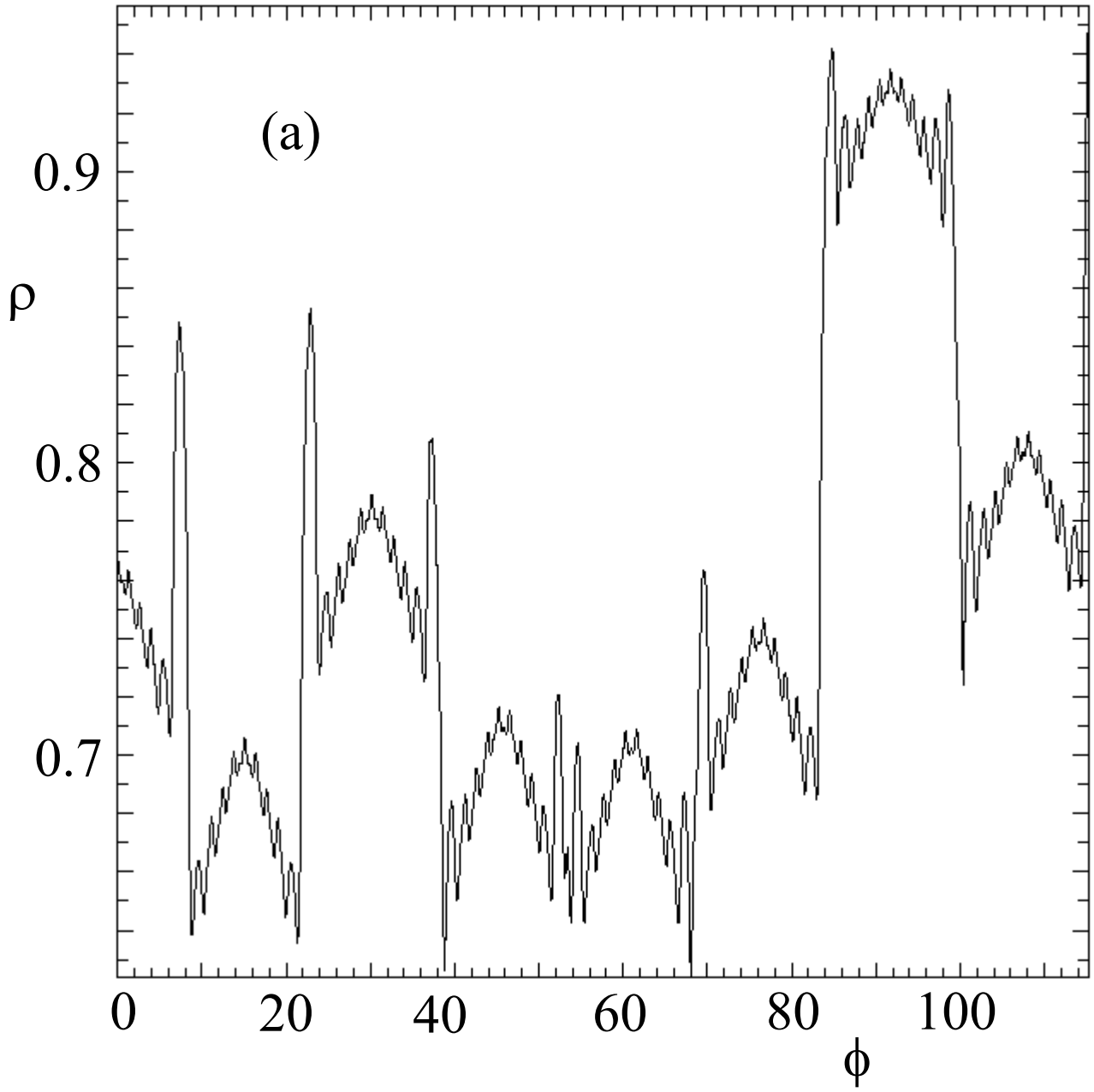

Fig. 4a

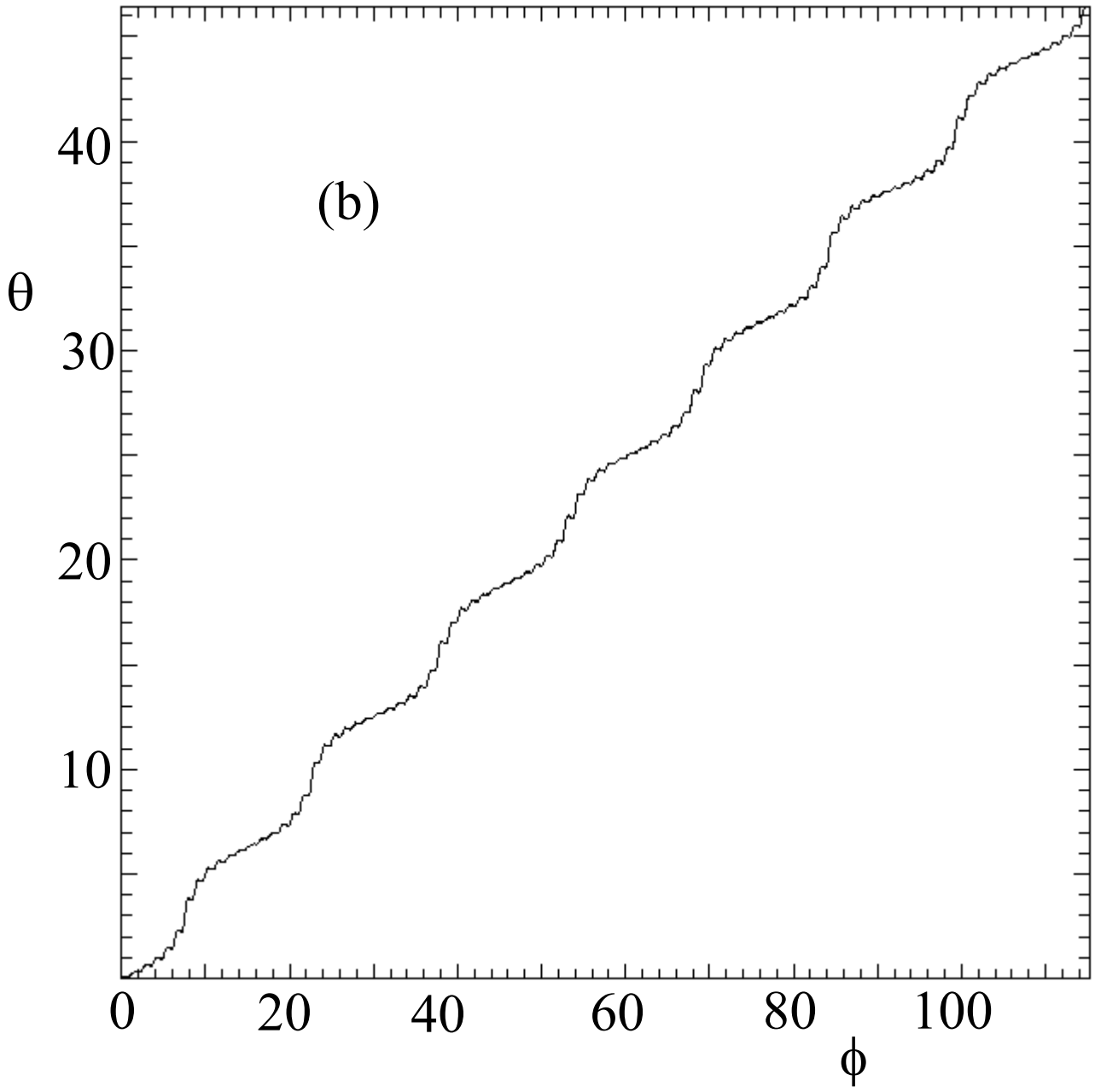

Fig. 4b

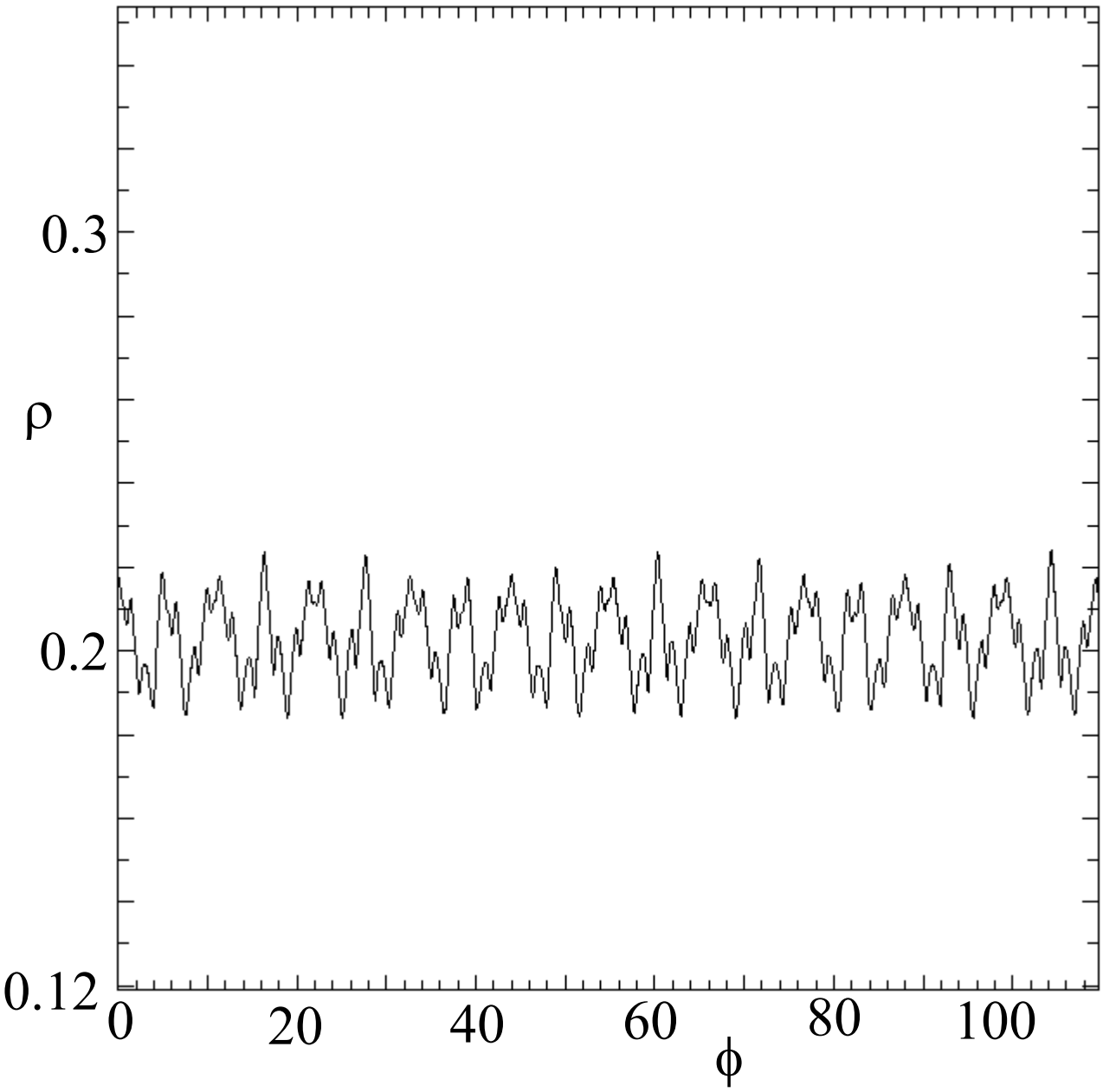

Fig. 5

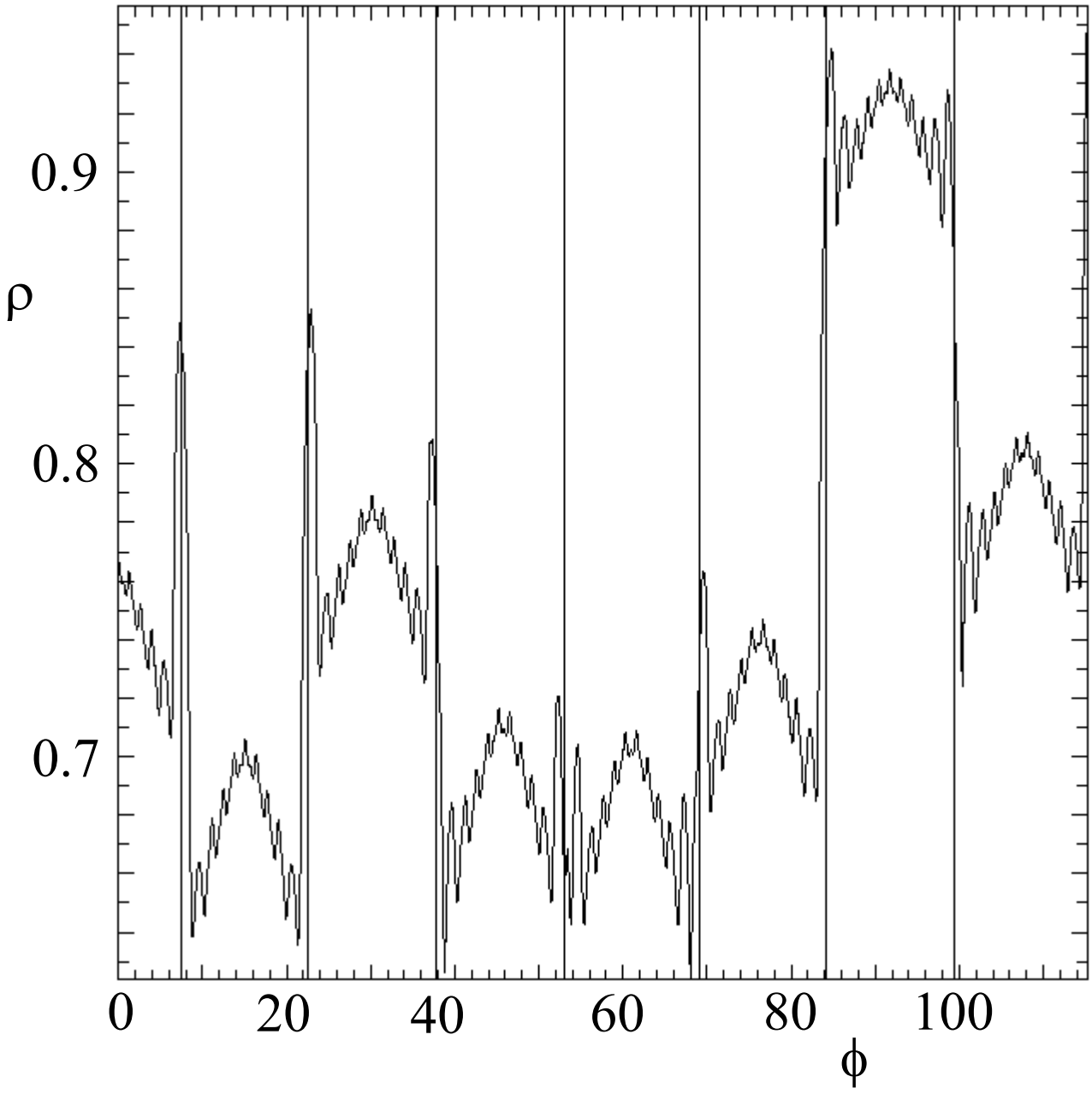

Fig. 6

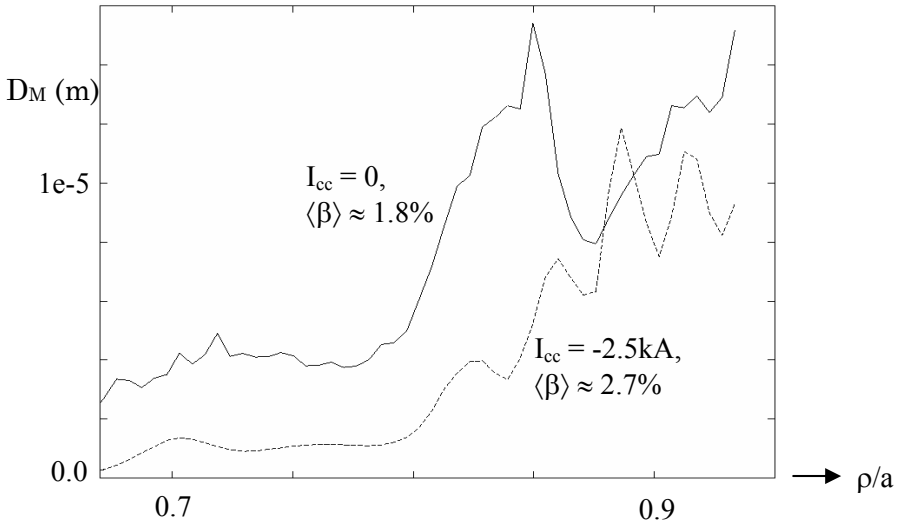

FIG. 7.

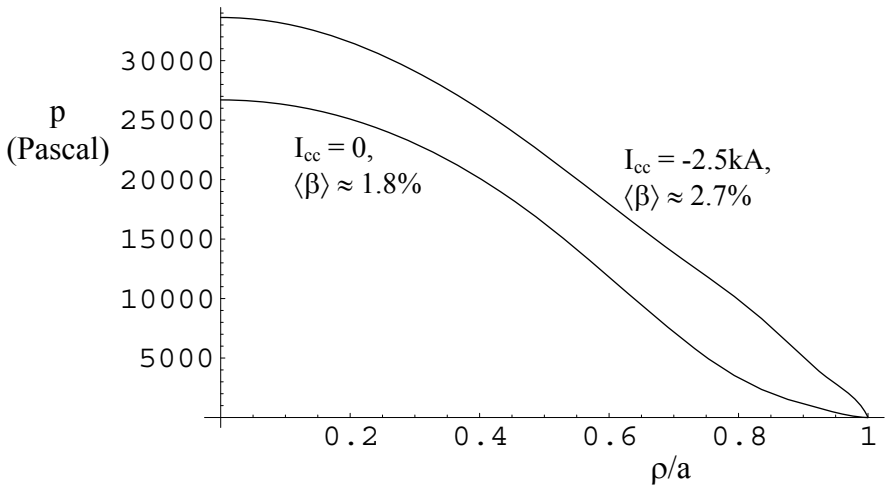
p
(Pascal)
30000
25000
20000
15000
10000
5000
0.2
0.4
0.6
0.8
1
ρ/a
I_{cc} = 0,
⟨β⟩ ≈ 1.8%
I_{cc} = -2.5kA,
⟨β⟩ ≈ 2.7%

FIG. 8.